

Sensitivity and resolution of proton detected spectra of a deuterated protein at 40 and 60 kHz magic-angle-spinning

Andrew J. Nieuwkoop · W. Trent Franks · Kristina Rehbein · Anne Diehl · Ümit Akbey · Frank Engelke · Lyndon Emsley · Guido Pintacuda · Hartmut Oschkinat

Received: 12 November 2014 / Accepted: 21 January 2015 / Published online: 8 February 2015
© Springer Science+Business Media Dordrecht 2015

Abstract The use of small rotors capable of very fast magic-angle spinning (MAS) in conjunction with proton dilution by perdeuteration and partial reprotonation at exchangeable sites has enabled the acquisition of resolved, proton detected, solid-state NMR spectra on samples of biological macromolecules. The ability to detect the high-gamma protons, instead of carbons or nitrogens, increases sensitivity. In order to achieve sufficient resolution of the amide proton signals, rotors must be spun at the maximum rate possible given their size and the proton back-exchange percentage tuned. Here we investigate the optimal proton back-exchange ratio for triply labeled SH3 at 40 kHz MAS. We find that spectra acquired on 60 % back-exchanged samples in 1.9 mm rotors have similar resolution at 40 kHz MAS as spectra of 100 % back-exchanged samples in 1.3 mm rotors spinning at 60 kHz MAS, and for (H)NH 2D and (H)CNH 3D spectra, show 10–20 % higher sensitivity. For 100 % back-exchanged samples, the

sensitivity in 1.9 mm rotors is superior by a factor of 1.9 in (H)NH and 1.8 in (H)CNH spectra but at lower resolution. For (H)C(C)NH experiments with a carbon–carbon mixing period, this sensitivity gain is lost due to shorter relaxation times and less efficient transfer steps. We present a detailed study on the sensitivity of these types of experiments for both types of rotors, which should enable experimentalists to make an informed decision about which type of rotor is best for specific applications.

Keywords Solid-state NMR · Fast spinning · Proton detection · Deuteration · ^1H back exchange

Introduction

Three-dimensional NMR spectroscopy correlating proton, carbon and nitrogen chemical shifts is an indispensable element of NMR structure determination protocols for biological macromolecules. Proton chemical shifts of proteins are strongly structure sensitive and hence well dispersed. As such, they represent a powerful, orthogonal parameter for resolving crowded spectra. Accordingly, assignment and restraint collection strategies utilizing proton chemical shifts are increasingly being used in magic-angle-spinning (MAS) NMR, despite technical challenges connected to the large proton linewidths caused by strong ^1H – ^1H interactions within the dense proton dipolar coupling networks of proteins. The number of dipolar interactions may be reduced by uniform deuteration and their magnitude decreased by very fast MAS and multiple pulse technologies.

Early studies using frequency-switched Lee–Goldburg techniques and carbon detection allowed the assignment of SH3 domain proton signals (van Rossum et al. 2001).

A. J. Nieuwkoop · W. T. Franks · K. Rehbein · A. Diehl · Ü. Akbey · H. Oschkinat (✉)
Leibniz-Institut für Molekulare Pharmakologie (FMP), Robert-Rössle-Strasse 10, 13125 Berlin, Germany
e-mail: oschkinat@fmp-berlin.de

F. Engelke
Bruker Biospin GmbH, Silberstreifen, 76287 Rheinstetten, Germany

L. Emsley · G. Pintacuda
Centre de RMN à très haut champ, Université de Lyon (CNRS/ENS Lyon/UCB Lyon 1), 5 rue de la Doua, 69100 Villeurbanne, France

L. Emsley
Institut des Sciences et Ingénierie Chimiques Ecole Polytechnique Fédérale de Lausanne (EPFL), 1015 Lausanne, Switzerland

Later, the combined approach of deuteration at non-exchangeable sites and partial reprotonation of amide moieties facilitated direct proton detection (Akbe et al. 2010; Chevelkov et al. 2003, 2006; Linser et al. 2008; Reif et al. 2001; Ward et al. 2011). These methods have since been progressively elaborated into more complex pulse schemes making use of faster spinning in the range of 40–60 kHz (Knight et al. 2011; Lewandowski et al. 2011; Marchetti et al. 2012; Zhou et al. 2006, 2007a) resulting in the design of solution NMR-like assignment strategies (Barbet-Massin et al. 2014; Chevelkov et al. 2014; Zhou et al. 2012), and 3D and 4D pulse sequences for determining the structure of proteins (Agarwal et al. 2014; Huber et al. 2011; Knight et al. 2012b; Linser et al. 2014; Zhou et al. 2007b). However, fundamental physical constraints limit the MAS rate possible for a given diameter of rotor. In turn, smaller diameter rotors with faster maximum spinning frequencies provide less space for protein material, limiting the sensitivity of experiments at higher MAS rates. On the other hand, improved filling factors, RF efficiencies, and the fundamental principles of MAS favor the smaller rotors.

Given the variety of rotor diameters that are currently available, the experimentalist is confronted with different upper limits of MAS rate and sample amount, which in turn dictate the appropriate pulse sequences, labeling, and ^1H back-exchange strategy to be used. While optimizing both sensitivity and resolution is the ultimate goal, in practice this may not be possible. Particularly in the context of the partial back-exchange of protons, sensitivity can be traded for resolution by lowering the ^1H back-exchange percentage. In this situation, it may make sense to pose a minimum acceptable resolution at which spectra of proteins in the 250 residue range may be conveniently evaluated, perhaps 50 Hz in the ^1H dimension, after which questions of sensitivity would be considered. The chosen compromise between resolution and sensitivity must also enable sufficient S/N in 3D spectra containing both ^{15}N – ^{13}C and ^{13}C – ^{13}C transfers. Spectra of 100 % back-exchanged samples packed in 1.3 mm rotors spun at 60 kHz MAS satisfy these requirements and serve as a useful benchmark for comparisons. Overall, optimal choices are not trivial and depend on the homogeneous and heterogeneous contributions to the linewidth, the effects of internal protein dynamics on MAS, as well as chemical exchange and T_2 requirements.

Since rotor dimensions limit the sample quantity and maximum spinning frequency, the degree of proton back-exchange that maximizes signal-to-noise and/or resolution is directly correlated with each rotor size. For rotors with ~ 24 kHz MAS limits (3.2 mm), ^2H labeling of the protein followed by back-exchange with ^1H at the labile sites to 10 % yields optimally resolved 2D spectra with proton linewidths around 10–18 Hz (Chevelkov et al. 2006). On

the other hand, optimal signal-to-noise was achieved between 30 and 40 % at the cost of increasing ^1H linewidths to 28 ± 6 Hz (Akbe et al. 2010). At 60 kHz spinning, full re-protonation to 100 % of the exchangeable sites still allows for narrow lines of signals from residues in the structured regions in samples of microcrystalline and non-crystalline medium-sized protein domains (Knight et al. 2011). An additional sharpening of the ^1H lines by a factor of two was seen in spectra of fully back-exchanged ubiquitin when increasing the MAS rate from 50 to 100 kHz (Agarwal et al. 2014). For experiments done using 1.3 mm rotors, sensitivity for spectra of a 100 % back-exchanged sample was seen to increase by a factor of about 2.5 between 40 and 60 kHz (Lewandowski et al. 2011). In two recent studies, spectra acquired using 1.3 mm rotors at 50–60 kHz MAS were seen to have similar sensitivity to spectra of 3.2 mm rotors spinning at 20 kHz, one using 25 % random protonation at all sites (Asami et al. 2012), the other 40 % ^1H back-exchange (Ward et al. 2014). This is despite the fact the sample volume for a 3.2 rotor is 30–40 μL compared to only 1.7 μL for 1.3 mm rotors. The 1.9 mm rotors also used in this study have sample volumes of 10 μL . So, while 60 kHz MAS or higher appears to be better in terms of decoupling dipolar ^1H – ^1H interactions, it remains to be seen whether sensitivity is maximized at faster MAS rates due to the requirement of smaller rotors with smaller sample volumes.

In this paper, we compare 2D and 3D spectra recorded with 1.9 and 1.3 mm probes in order to analyze the factors determining signal-to-noise and resolution, including the level of ^1H back-exchange and MAS rate. As a starting point, 2D (H)NH spectra were acquired on samples of triply ($^2\text{H}^{13}\text{C}^{15}\text{N}$) labeled SH3 back-exchanged at the labile sites with 100 % $^1\text{H}_2\text{O}$ using a 1.9 mm rotor at 40 kHz MAS (Fig. 1, red) and a 1.3 mm rotor at 57 kHz MAS (Fig. 1, blue). The spectrum acquired on the 1.9 mm rotor at 40 kHz was 2.7 times more sensitive (318 ± 164 vs. 115 ± 61 S/N/Hr), while the spectrum from the faster spinning 1.3 mm rotor yields ^1H linewidths that are twice as sharp (42 ± 15 vs. 87 ± 21 Hz).

The large variations in signal-to-noise and linewidth seen in Fig. 1 are indicative of the fact that SH3 contains both well-ordered and extremely mobile domains, which have different cross-polarization and relaxation behaviors (Lewandowski et al. 2011). To enable the analysis of how the signals of residues with different dynamics, and hence different relaxation behavior, are affected by MAS rates and deuteration level, three groups of residues were selected on the basis of ^1H T_2 values. These T_2 values were determined site specifically, to be discussed in detail later, from spectra acquired on a 100 % back-exchanged sample at 60 kHz MAS. The residues selected for the “best” group (Q16, M25, F52, K60) come from rigid strands and their

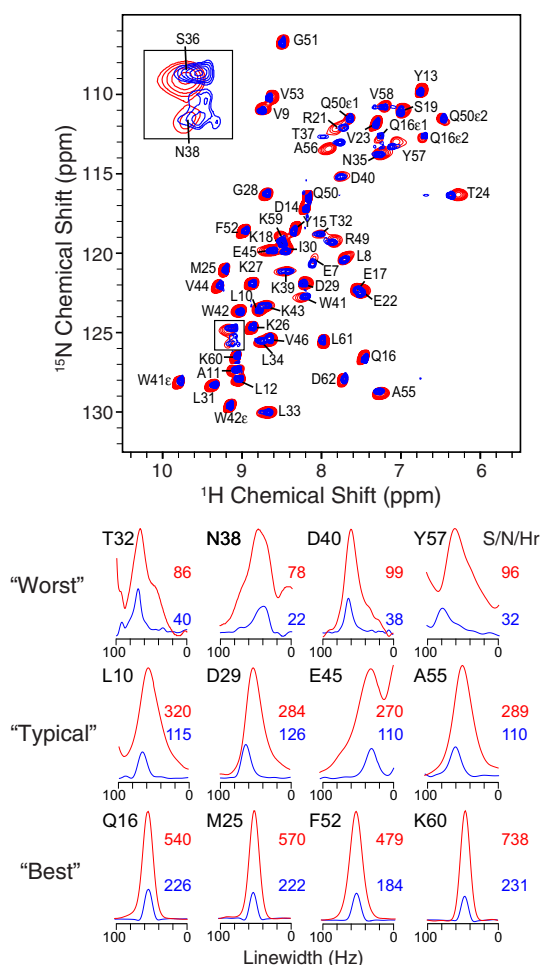


Fig. 1 (H)NH 2D of $^2\text{H}^{13}\text{C}^{15}\text{N}$ labeled SH3 back-exchanged to 100 % using a 1.3 mm rotor spinning at 57 kHz (blue) and 1.9 mm rotor spinning at 40 kHz (red). Peaks are labeled with their assignment; all peaks are amide backbone unless labeled with an appropriate side chain letter. 1D slices of selected residues from the three T_2 classes are shown, scaled relative to the 1.9 mm data to illustrate the sensitivity differences between the two modules. The signal to noise per hour for each peak is listed to the right. Spectra were acquired at 600 MHz. The VT set point was 260 K

signals have ^1H T_2 values of >30 ms. Those picked for the “typical” group (L10, D29, E45, A55) are at the edge of beta-strands or part of the structured alpha-turn and give signals with ^1H T_2 values of 10–15 ms (near the median value of 14 ms). The residues in the “worst” class are from mobile loops (T32, N38, D40, Y57) and ^1H T_2 values of 6–8 ms were observed. Extracted 1D slices for the peaks of all twelve residues are shown in Fig. 1 to illustrate their resolution and intensity differences. At 100 % back-protonation, the peaks of the “best” class residues have similar ^1H linewidths at both 40 and 60 kHz MAS, while the signals for the “typical” and “worst” class residues are narrower at the faster MAS rate. By comparing the sensitivity and resolution of 2D (H)NH and 3D (H)CNH- and

(H)C(C)NH-type experiments, with a focus on these three groups of residues, we were able to investigate how faster spinning and lower ^1H back-exchange percentages affect the acquisition of the data needed to perform sequential assignments.

Materials and methods

NMR spectroscopy

NMR experiments were performed on Bruker Avance II and III spectrometers with ^1H Larmor frequencies of 600, 900 and 1,000 MHz. At 600 MHz, 1.3 mm (^1H - ^{13}C - ^{15}N) triple resonance and 1.9 mm (^1H - ^{13}C / ^{15}N) double resonance probes were used. At 900 MHz, 1.9 mm quadruple (^1H - ^{13}C - ^{15}N - ^2H) resonance and at 1,000 MHz, 1.3 mm triple (^1H - ^{13}C - ^{15}N) resonance probes were used. 2D (H)NH type experiments using cross polarization and MISSISSIPPI solvent suppression were used for all samples and probes (Zhou and Rienstra 2008). On the 1.9 mm rotors (H)CNH- and (H)C(C)NH-type experiments, *e.g.* (H)CANH and (H)CA(CO)NH 3Ds (the nuclei listed in parenthesis were used for transfers but not detected), were acquired using previously published pulse sequences (Barbet-Massin et al. 2014; Zhou et al. 2012) using tangent ramped cross polarization for ^1H - ^{15}N , ^1H - ^{13}C and ^{13}C - ^{15}N transfers (Baldus et al. 1998; Hediger et al. 1993) and either DREAM (Verel et al. 2001) or INEPT (Kay et al. 1990) based ^{13}C - ^{13}C transfers. ^1H - ^{15}N and ^1H - ^{13}C conditions were optimized to just above $\omega_1^{\text{H}} = 3\omega_r/2$; $\omega_1^{\text{X}} = 1\omega_r/2$. ^{15}N - ^{13}C specific CP conditions were optimized between $\omega_1^{\text{C}} = 3\omega_r/4$; $\omega_1^{\text{N}} = 1\omega_r/4$ and $\omega_1^{\text{C}} = 5\omega_r/4$; $\omega_1^{\text{N}} = 1\omega_r/4$. In both cases RF limitations on the ^{13}C and ^{15}N channels prevented the use of higher power conditions. Higher CP transfer efficiencies may be possible with improved RF performance. ^1H decoupling was done with WALTZ-16 (Shaka et al. 1983) or sITPPM (Lewandowski et al. 2010) during all indirect evolution periods. WALTZ-16 ^{13}C and ^{15}N decoupling was applied during acquisition. Rotors were sealed with silicon rubber disks to prevent the loss of solvent during spinning. For the experiments at 600 MHz the variable temperature gas was set to 260 K, at 900 MHz to 240 or 260 K, and at 1,000 MHz to 235 K. According to external calibration with ethylene glycol or polyethylene glycol, this corresponds to sample temperatures of 296 and 304 K respectively, for the 900 MHz, and 299 K for the 1,000 MHz spectra. No calibration for the 600 MHz data is available, however, similar VT gas temperature and flow parameters on the 900 MHz spectrometer resulted sample temperatures of 315 K at 40 kHz MAS.

Sample preparation

SH3 samples were expressed and purified as discussed previously (Akbej et al. 2010), with the exception that $^1\text{H}/^2\text{H}$ exchange was performed at pH 3.5, in the presence of ammonium sulfate. In brief, the chicken α -spectrin SH3 domain was expressed in *E. coli* BL21-DE3 grown in 100 % $^2\text{H}_2\text{O}$ with M9 minimal medium containing 3 g/L of d_7 - ^{13}C -glucose, 1 g/L ^{15}N -ammonium chloride, and 60 mg/L carbenicilline. Cells from 0.2 L of overnight culture in $^1\text{H}_2\text{O}$ were used to inoculate 1 L of expression culture. Cells were grown to an $\text{OD}_{600\text{nm}}$ of 0.7 at 37 °C and then induced at 20 °C with 1 mM IPTG overnight. After purification of the tagless protein by anion exchange chromatography (Q-Sepharose FF) and gel filtration (Superdex 75), the protein was lyophilized and redissolved in $^1\text{H}_2\text{O}/^2\text{H}_2\text{O}$ mixtures of 60, 80, and 100 % $^1\text{H}_2\text{O}$. An equal volume of 200 mM ammonium sulfate solution at the appropriate $^1\text{H}_2\text{O}/^2\text{H}_2\text{O}$ ratio was added and samples were stored at 4 °C for at least 3 days to ensure exchange. Crystallization was initiated via a pH shift to 7.5 ± 0.5 under an NH_3 atmosphere. Microcrystals were packed into 1.3 or 1.9 mm rotors using a table-top centrifuge (Eppendorf 5417-F).

Results and discussion

Comparing the relative effectiveness of the 1.9 and 1.3 mm probes first requires determining the optimal conditions for ^1H -detection at 40 kHz MAS. The first step in this process was to identify at which level of ^1H back-exchange the proton linewidths were sufficiently narrow in spectra at 40 kHz MAS. As such, (H)NH 2D spectra of triply labeled

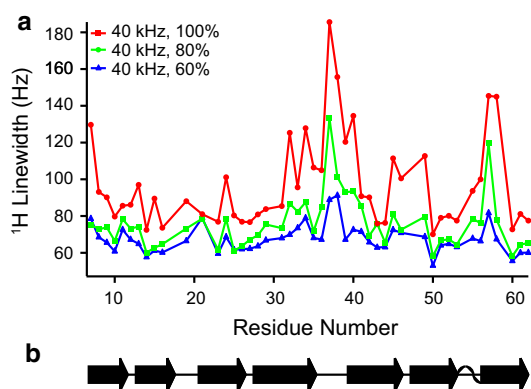


Fig. 2 ^1H linewidths based on ^1H back-exchange percentage at 40 kHz MAS. Linewidths (a) measured from (H)NH 2D spectra acquired at 40 kHz MAS on a 1.3 mm probe at 600 MHz. Samples were back-exchanged with 100 % (red) 80 % (green) or 60 % (blue) $^1\text{H}_2\text{O}$ prior to crystallization. Secondary structure elements are indicated in (b)

SH3 samples, back-exchanged to 100, 80 and 60 % protons at the labile sites, were acquired and the ^1H linewidths (Fig. 2) analyzed.

In general, linewidths of the signals from residues in the regions with well-defined secondary structure, as determined from the crystal structure (pdb ID: 1U06, Fig. 2b) (Chevelkov et al. 2005), are narrower than those in the flexible turns and loops. Spectra acquired on samples with lower ^1H back-exchange percentages have sharper linewidths for the peaks of all residues, but most dramatically for those in the mobile regions. A similar sharpening effect for peaks of these residues was observed previously in SH3 with increasing MAS rates (Lewandowski et al. 2011). At 60 % back-exchange, the ^1H linewidths for peaks from the mobile regions narrowed to the values observed for the other signals of the protein and bulk ^1H T_2 values reached those seen for a 100 % sample at 60 kHz (15 ms T_2). By comparing three conditions: (1) a 1.9 mm rotor with a 100 % back-exchanged sample spinning at 40 kHz (1.9/100 %), (2) a 1.9 mm rotor with a 60 % back-exchanged sample spinning at 40 kHz (1.9/60 %) and (3) a 1.3 mm rotor spinning at 60 kHz containing a 100 % back-exchanged sample (1.3/100 %), the effects of module size—and therefore MAS rate and material amount—and ^1H back-exchange level on sensitivity and resolution was then investigated.

The ultimate goal of lowering the ^1H back-exchange percentage or increasing the MAS rate is to decrease R_2 relaxation rates and as a result increase resolution as well as sensitivity in multidimensional/multi-transfer experiments. To gain a detailed understanding of the benefits of and differences between faster spinning and ^1H dilution, site-specific ^{15}N and ^1H R_2 rates were determined through the use of 2D (H)NH correlation experiments combined with an echo period immediately prior to ^{15}N evolution or ^1H acquisition. Peak intensities were extracted from 2D planes at multiple echo times and the R_2 relaxation rates for residues with sufficiently intense and resolved peaks were determined by fitting in CCPN Analysis (Stevens et al. 2011).

In Fig. 3, R_2 relaxation rates for ^{15}N (Fig. 3a) and ^1H (Fig. 3b) are plotted by residue number for the 1.3/100 % (blue), the 1.9/100 % (red) and the 1.9/60 % (green) samples. In all three cases, R_2 rates for the signals of residues in the loop regions around residues 21, 38 and 58 were higher than for the residues in regions with well-defined secondary structure. Both faster spinning and ^1H dilution cause relaxation rates for the signals of residues in the loops to regions to decrease, approaching values observed for the signals of residues in the structured core of the protein: 10–15 s^{-1} for ^{15}N and 20–80 s^{-1} for ^1H . Average R_2 rates for the signals of all amide sites are very similar for the 1.9/60 and 1.3/100 % samples, 70 and

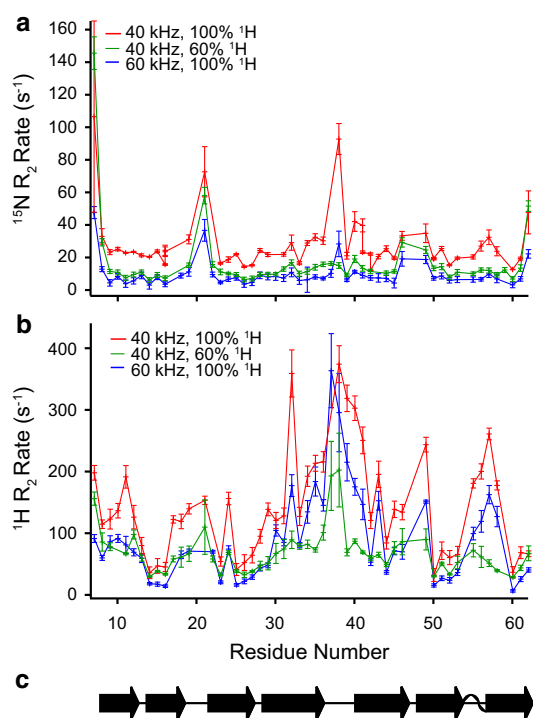


Fig. 3 Site-specific R_2 relaxation rates for **a** ^{15}N and **b** ^1H measured at MAS rates of 40 kHz on the 1.9/100 % sample (red) and 1.9/60 % sample (green) and at 60 kHz on the 1.3/100 % sample (blue). 40 kHz data were acquired at 900 MHz ^1H frequency and 60 kHz data at 1,000 MHz. Error bars indicate the standard deviation of the fit value, determined via covariance fitting in CCPN Analysis. Secondary structure elements are indicated in (c)

89 s^{-1} and for ^{15}N and 17 and 16 s^{-1} for ^1H in the 1.9/60 and 1.3/100 % samples respectively. In fact, for the residues in the mobile regions ^1H dilution appears to be more effective at decoupling protons than faster spinning, as ^1H R_2 rates are lowest for the signals of the 1.9/60 % sample (Fig. 3b), note that for T37 no R_2 value could be determined for the 1.9/100 % sample, causing the blue and red lines to intersect. This is consistent with internal protein dynamics interfering with the effects of MAS, which for more rigid regions yield a linear improvement in linewidth as MAS rate is increased. As a result, for proteins with more internal motions, for example membrane proteins in a lipid environment, lower protonation levels might be beneficial, even at 60 kHz MAS. A similar trend for the signals from the loop regions is not seen for the ^{15}N R_2 rates, (Fig. 3a) where the rates are the lowest for the 1.3/100 % sample at all sites with the exception of N38. This discrepancy relative to the ^1H rates could have several causes. One difference is the use of RF based ^1H - ^{15}N decoupling while the ^1H - ^1H decoupling relies entirely on the MAS. In addition, all ^{15}N sites observed are protonated, which means any dilution effects are long-range. Finally, ^1H - ^{15}N dipolar couplings are ten times weaker, at a given

distance, than ^1H - ^1H couplings and are thus more easily decoupled with respect to the MAS rates used.

Having established that the R_2 rates for signals in spectra of the 1.9/60 and 1.3/100 % samples are similar or slower than those of signals from the 1.9/100 % sample, it now remains to be seen how this will affect sensitivity and resolution. Recall that in Fig. 1, for samples at 100 % back-exchange, spectra acquired on 1.9 mm rotors had more signal, but worse resolution, than those acquired on 1.3 mm rotors. To assess if this situation was improved for 60 % back-exchanged samples, and to check on the effects/importance of the individual balance between line width and sample amount for the two 100 % samples, 2D (H)NH, 3D (H)CNH- and 3D (H)C(C)NH-type experiments were acquired at 900 MHz for the 1.9/100 and 1.9/60 % samples and at 1,000 MHz for the 1.3/100 % case. The signal-to-noise values for peaks in the 2D and 3D spectra associated with the residues in the three T_2 classes selected earlier are displayed in Fig. 4.

Similar to what is displayed in Fig. 1, (H)NH 2D spectra are more sensitive on the 1.9/100 % sample than the 1.3/100 % sample (Fig. 4a). The ratio is 2.4:1 for the signals of residues with the “best” T_2 values, and falls to 1.6:1 and 1.7:1 for those signals with “typical” and “worst” T_2 values, respectively. The average for the signals of all backbone amide sites is 1.9:1. Thus for (H)NH experiments, the signals of the “best” residues have noticeably higher sensitivity while the behavior of those in the other two classes are more similar to the protein overall. Comparing the signals in the spectrum of the 1.9/60 % sample to those in the spectrum of the 1.3/100 % sample the overall ratio was 1.2:1, with similar behavior across all residue classes.

Interestingly, in the (H)NH 2D spectra the ratio between the signals from the 1.9/60 and 1.9/100 % samples is 52 % for those residues with the “best” T_2 values. After accounting for the slightly larger amount of material in the 100 % rotor, it follows that ^1H dilution gives minimal benefit for the signals from these residues due to the fact the R_2 rates for these sites were already very slow (Fig. 3b). For signals of residues with “typical” T_2 times the ratio is 62 %, and for the “worst”, it is 82 %; again consistent with the fact these residues showed improved R_2 rates on the 1.9/60 % sample. This trend would not have been observed without a site-specific analysis since the average ratio for the signals of all amide sites was 60 %, which follows the percentage of sites that are labeled. Therefore, in contrast to observations at 24 kHz MAS, lower ^1H back-exchange levels do not yield higher overall signal in (H)NH 2Ds at 40 kHz for SH3, but rather serve to increase resolution. However, in samples with more dynamics, ^1H dilution might result in greater sensitivity gains.

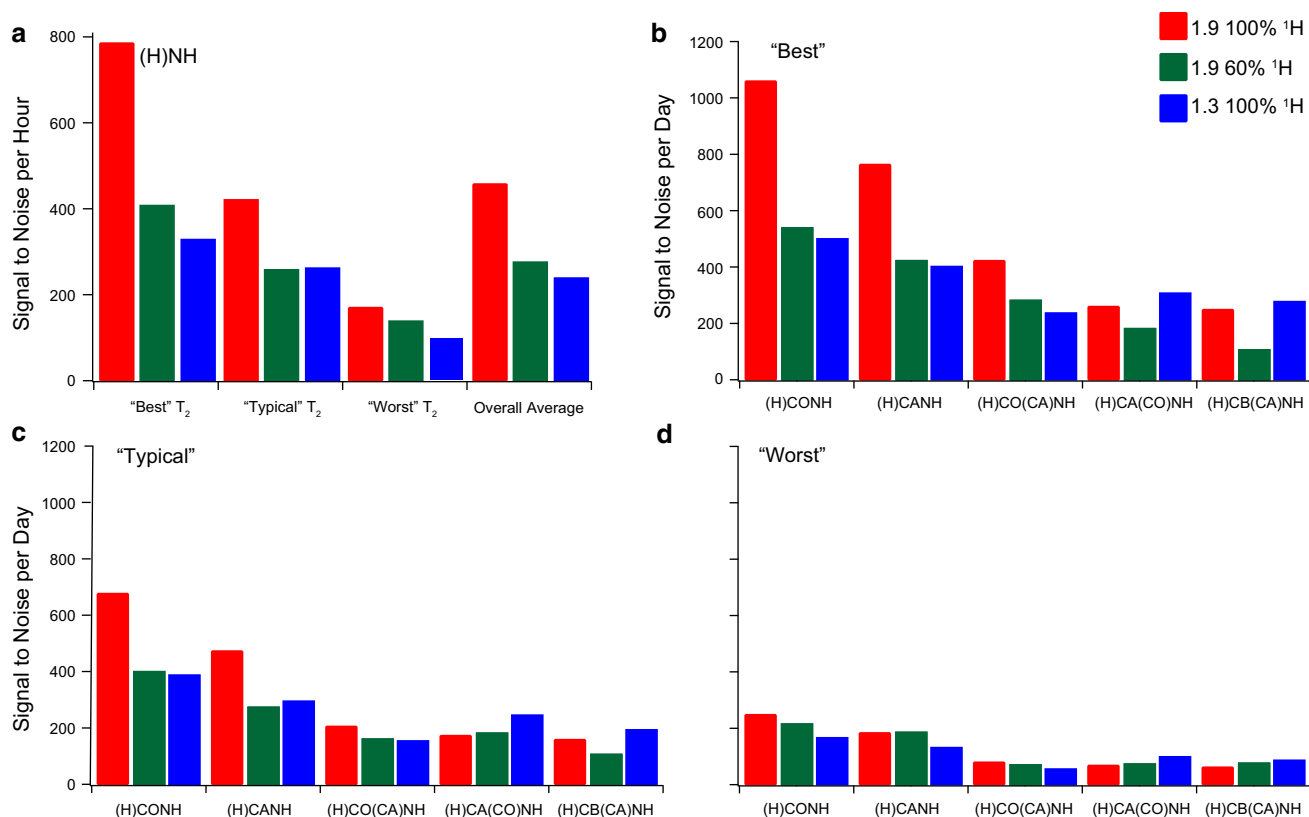


Fig. 4 Signal-to-noise of 2D and 3D experiments acquired on 1.9 and 1.3 mm rotors. The comparison between a 100 % back-exchanged sample in a 1.9 mm rotor spinning at 40 kHz (red), a 60 % back-exchanged sample in a 1.9 mm rotor spinning at 40 kHz (green), and a 100 % back-exchanged sample in a 1.3 mm rotor spinning at 60 kHz (blue). Sensitivity was measured for three classes of residues: those with the best T_2 times (Q16, M25, F52, K60), those with typical

T_2 times (L10, D29, E45, A55), and those with the worst T_2 times observed (S36, N38, K43, Y57). The signal-to-noise per day in an (H)NH 2D experiment is shown in (a) for the three classes and also the average for all residues. Signal-to-noise per day averaged for 3D experiments for the “best” (b) “typical” (c) and “worst” (d) residue classes

When considering the sensitivity of the 3D spectra, all experiments were processed so that equal acquisition times were considered in all dimensions. This resulted in broader but also more sensitive peaks for some experiments, especially on the 1.3/100 and 1.9/60 % samples. For example, when processing the (H)CONH 3D spectra for Fig. 4, points that span 10 ms of evolution in the ^{15}N indirect dimension were used. For the 1.3/100 % sample, 20 ms of points had been collected. As a result the average ^{15}N linewidth for signals in the spectrum increased to 78 ± 4 from 38 ± 3 Hz, with the average S/N/day rising to 344 ± 144 from 270 ± 105 . This illustrates the resolution benefits which can be gained from longer indirect dimension acquisition times at a very moderate cost in sensitivity, made possible by the very long ^{15}N T_2 times observed for the signals in these samples.

The data from the 3D (H)CNH-type experiments for the three classes of T_2 values (Fig. 4b–d) shows that signals from the 1.9/100 % sample have a ratio in signal-to-noise per day of 1.8:1 relative to signals from the 1.3/100 %

sample, showing a somewhat attenuated advantage for the 1.9 mm module as compared to what was seen for the (H)NH 2D spectra. Meanwhile the 1.9/60 % sample yields a ratio of 1.1:1, again only a slight decrease to from what was seen for the (H)NH. ^{15}N – ^{13}C transfer efficiencies, as calculated from the sensitivity of the average of the two (H)CNH experiments divided by the (H)NH, do not vary substantially over the three samples, with values of 38, 35 and 35 % for the 1.3/100, 1.9/100 and 1.9/60 % respectively. Note the measured ^{15}N T_2 values for the signals of all samples were above 50 ms and thus not a factor for sensitivity differences amongst samples. The sensitivity of the (H)CONH is in all cases greater than the (H)CANH as a result of the better CO–N SPECIFIC CP transfer, but perhaps also due to the differences in CO and CA T_2 values, which will be discussed more below.

When C–C transfers are additionally employed, i.e. in the (H)C(C)NH-type 3Ds, the signal-to-noise of spectra acquired for both the 1.3/100 % sample relative to the 1.9/100 %, and for the 1.9/60 % sample relative to the 1.9/

100 % increases due to the lower R_2 relaxation rates. The ratio for signal-to-noise per day, averaged for the (H)CA(CO)NH and (H)CO(CA)NH spectra, acquired on the 1.9/100 and 1.3/100 % samples was to 1:1. For the 1.3/100 % samples, an improved (H)(CO)CA(CO)NH sequence was used, which shifts this value in favor of the 1.3/100 % samples slightly. For the “best” T_2 class residues, the ratio was 1.1:1, while for the “typical” and “worst” T_2 values the ratio was 0.9:1. The comparison between the signals for the 1.9/60 and 1.3/100 % samples shows a ratio of 0.9:1 for all three T_2 classes. So, in contrast to what was seen for the (H)NH and (H)CNH-type experiments, the relative sensitivity of experiments with C–C mixing of the 1.9/100 and 1.9/60 % samples yields a value significantly higher than 60 % of amide sites protonated. The overall average for all backbone amide signals was 84 %. This breaks down to 75 % for the “best” T_2 class, 96 % for the signals from “typical” T_2 value residues and 102 % for the “worst”. As more complicated proteins are likely to have T_2 values more similar to those of the “worst” or “typical” sites in SH3, these values (Fig. 4c, d) are the most relevant to consider for future experiments.

An additional variable to be considered is that various methods have been developed for acquiring such suites of spectra for site-specific assignments. They differ primarily in their use of scalar and/or dipolar based transfer schemes, ranging from solution-like experiments based purely on scalar transfers (Linser et al. 2008), to exclusively dipolar interaction-mediated transfer sequences with CP based H–N and N–C transfers including DREAM based C–C transfers (Zhou et al. 2012) and further to ‘combination sequences’ with CP based H–N and N–C transfers and INEPT based C–C transfers (Barbet-Massin et al. 2013; Knight et al. 2011). As scalar coupling based C–C transfers require a relatively long echo period, optimally 18.8 ms for CA–CO and 28.8 ms for CB–CA, sufficiently long aliphatic T_2 times are required for them to be efficient. Therefore, due to the fact ^2H – ^{13}C interactions are currently only decoupled by MAS, the efficiency for 3D experiments at 60 kHz relative to 40 kHz MAS for 100 % samples was much improved. A single J-based CA–CO transfer on the 1.9/100 % sample—taken as the average signal in the (H)C(C)NH-type experiments relative to the (H)CNH-type—was 35 % efficient on average, while at 60 kHz the efficiency was 58 %. For the 1.9/60 % sample the value rose to 44 %. This was slightly better than the average efficiency for the DREAM based transfers, which were around 30 % (data not shown). However the longer echo needed for the CB–CA transfer meant that DREAM was more efficient at 40 kHz. For the 1.9/60 % sample, the bulk CO T_2 was measured to be at least 80 ms while the T_2 of the CA signal was 20 ms. Therefore, one can envision that the addition of ^2H decoupling to remove the ^2H – ^{13}C

interactions and increase the CA T_2 would improve the efficiency of scalar coupling based mixing at 40 kHz.

To determine the amount of labeled material in each rotor, direct excitation ^{13}C spectra were acquired which, after comparison to spectra of a known amount of natural abundance glycine, indicated there is 1.8 mg of protein in the 1.3/100 % sample, 9.9 mg in the 1.9/100 %, and 8.2 mg in the 1.9/60 % rotor. When compared with the total masses of material packed: 2.3, 12.9 and 10.4 mg respectively, we can conclude that 75 % of the mass of the sample in each rotor is protein with the rest being water and precipitant. 1D proton spectra of the samples indicate the presence of different amounts of free water, especially in the 1.9 mm samples, which might be possible to remove through centrifugation as shown by Bockmann et al. (2009). Thus, the 1.3 mm probe yields far more signal per mg of sample, while the 1.9 mm probe yields more signal overall for (H)NH and (H)CNH-type experiments, and similar signal for (H)C(C)NH-type experiments.

Having addressed their relative sensitivity, the final question of the differences in spectra of the 1.3/100 and 1.9/60 % samples is their resolution. A comparison of 2D (H)NH spectra of the 1.3/100 % sample acquired at 1,000 MHz (blue) and the 1.9/60 % sample acquired at 900 MHz (red) is shown in Fig. 5.

As expected from the R_2 rates reported in Fig. 3 the overall resolution of the spectra is very similar, with an average ^1H linewidth of 56 ± 15 Hz for peaks in the 1.3/100 % spectrum (Fig. 5, blue) and 44 ± 13 Hz for the spectrum of the 1.9/60 % sample (Fig. 5, red). 1D slices of the peaks of the residues defining the three T_2 classes are shown below the spectra. The signals from the “worst” T_2 class residues are noticeably sharper in the spectrum of the 1.9/60 % sample than those in the spectrum of the 1.3/100 % sample, as expected from the ^1H R_2 rates. Additional peaks can be seen in the 1.9/60 % 2D spectrum, including the amide site of G5 as well as the side chain peaks for N35 and N47. Peaks from these extremely mobile residues were previously observed in INEPT based (H)NH 2D spectra, which enabled their assignment (Linser et al. 2010). Additionally, a peak observed in both spectra at a ^{15}N chemical shift between the signals from S36 and N38 (expansion Fig. 5) can be resolved in these high field spectra with 50 ms ^{15}N acquisition and was tentatively assigned as K6 based on its N and CA chemical shifts. The only 3D spectra which contained a peak at this resonance was the (H)CANH spectrum acquired on the 1.9/100 % sample, the 3D spectrum with the highest sensitivity for the i-residue of the recorded set. Isotope effects for the amide side chain peaks of Q16 and Q50 result in a peak doubling at those sites. Comparing the relative intensity of the NH_2 to the NHD peaks provided an internal check of the ^1H back-exchange percentage.

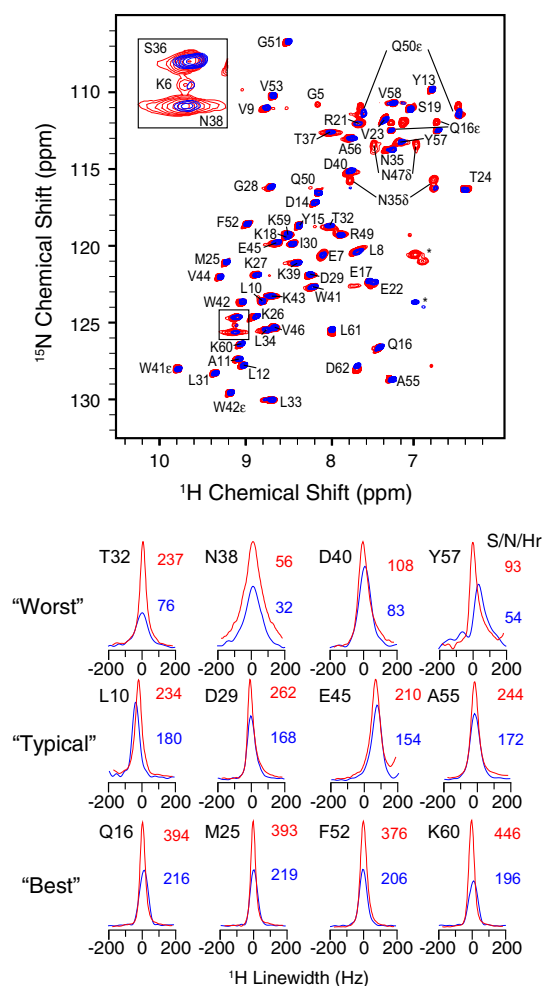


Fig. 5 (H)NH 2D spectra of 100 % back-exchanged SH3 at 60 kHz MAS (blue) and 60 % back-exchanged SH3 at 40 kHz MAS (red). 60 kHz spectrum was collected at 1,000 MHz ^1H frequency, while the 40 kHz spectrum was collected at 900 MHz. Peaks are labeled with their assignment, all peaks come from amide backbone sites unless labeled with a sidechain nitrogen letter. Two folded peaks are indicated with stars and do not overlay due to different acquisition windows. 1D traces of selected peaks from the three T_2 classes are shown, scaled relative to the 1.9 mm peaks. The data for this figure were processed to demonstrate achievable resolution. The relative sensitivity and resolution of each site can be compared with signal to noise per hour for each peak listed to the right, which due to the inclusion of more points in the ^{15}N dimension do not correlate exactly with those in Fig. 4. The calibrated sample temperature for the 60 kHz spectrum was 299 K, while the 40 kHz spectrum was at acquired at 304 K

As the resolution seen in the two spectra in Fig. 5 is extremely similar, a more detailed analysis of the associated linewidths, as well as a comparison to the linewidths observed in spectra acquired on the 1.9/100 % sample, is warranted. Table 1 contains the ^1H linewidths for peaks of the residues in the three defined groups, using identically processed (H)NH spectra of all three samples.

The average amide proton linewidths per group are sharpest for peaks in the spectrum of 1.9/60 % sample,

while those from the 1.3/100 % sample are slightly broader and those of the 1.9/100 % sample the broadest, in line with the data shown in Figs. 1 and 5. However the different trends seen for the peaks of the residues in the three T_2 classes tells a more interesting story. For spectra taken on 1.9 mm rotors there is a clear trend of increasing linewidths as you move from the best T_2 class to the worst, indicating differences for the three different regimes at this spinning rate. For the 1.3 mm sample on the other hand, the linewidths for the peaks of residues with the “best” and “typical” T_2 values are very similar, while for peaks of the “worst” residues a noticeable difference in linewidth appears. Moving down the table within the classes, we note that linewidths for the peaks of the “best” T_2 class residues are relatively constant (0.04–0.05 ppm). For residues in the “typical” T_2 class, linewidths for peaks from the spectrum of the 1.9/100 % sample stand out as noticeably broader, while those for the 1.9/60 and 1.3/100 % samples are similar. Finally, in the case of the worst T_2 residues, there is clear improvement from the 1.9/100 % to the 1.3/100 % and then again improvement in the spectrum of the 1.9/60 % sample. This once again points towards ^1H dilution as more effective at sharpening proton linewidths than faster spinning for the peaks of residues in mobile regions.

An alternative explanation for differences in linewidths could be the sample temperature. Data on the 1.3/100 % sample were acquired with a VT set point of 235 K, which was experimentally determined to result in a sample temperature of 299 K. For the 1.9/100 % data, the VT set point was 240 K, which was determined to be a sample temperature of 296 K, while for the 1.9/100 % the set point was 260 K, yielding a sample temperature of 304 K. Slight variations in chemical shifts in Fig. 5, for example for E22 and L61, are likely a result of these small differences. In contrast, due to hardware limitations, the VT set point for both the 1.3 and 1.9 mm probes was 260 K during the acquisition of the data shown in Fig. 1 taken at 600 MHz. Due to a lower flow rate this likely corresponds to a sample temperature of ~ 315 K for the 1.9 mm sample and even higher for the 1.3 mm. This resulted in much larger chemical shift differences, as can be seen in the expansions of Fig. 1. Consequently, we believe that for the data acquired on the 900 and 1,000 MHz spectrometers—on which all of the quantitative comparisons (Figs. 3, 4, 5; Table 1) were made—sample temperatures were very similar, and the linewidth differences observed are almost entirely a result of MAS and ^1H back-exchange differences.

Conclusions

We have shown that the resolution of SH3 2D spectra acquired on 60 % back-exchanged samples spinning at

Table 1 ^1H linewidths for (H)NH spectra

Sample	Field (MHz)	^1H linewidths (Hz)			
		Best T_2	Typical T_2	Worst T_2	All residue average
1.9/60 %	900	35	43	66	45 ± 16
1.3/100 %	1,000	48	50	80	56 ± 16
1.9/100 %	900	46	74	117	80 ± 35

40 kHz is extremely similar to that observed at 60 kHz MAS and 100 % protonation. However, the signal-to-noise in these spectra did not surpass that of a 100 % sample at 40 kHz in a 1.9 mm rotor. For two [(H)NH] and three [(H)CNH-type] transfer experiments, the spectra of the 100 % sample using a 1.9 mm rotor showed two to three times more sensitivity than the 1.3 mm rotor, while requiring about five times as much protein material. With the addition of a carbon–carbon transfer [(H)C(C)NH-type experiments] this gain in sensitivity dropped to between 0.7 and 1.5. The 1.9 mm rotor using a 60 % back-exchange sample showed ratios to the 1.3 mm rotor of 1.2:1 for the (H)NH, 1.1:1 for the (H)CNH-type 3Ds, and 0.8:1 for the (H)C(C)NH-type experiments. It is worth noting that for the residues with the “worst” T_2 values, these ratios increase to 1.4:1 for the (H)NH and (H)CNH-type 3Ds, and 0.9:1 for the (H)C(C)NH-type experiments. ^2H excitation followed by ^2H – ^{13}C CP (Akbe et al. 2014) may improve sensitivity for all experiments starting on deuterated carbons, especially on samples with less than 100 % back protonation or where ^1H back-exchange might be hampered. Similarly, ^2H – ^{13}C decoupling might improve the performance for all experiments (Huber et al. 2012), but it should be particularly beneficial for experiments acquired at 40 kHz MAS on the 1.9 mm probe, where a relatively short CA T_2 is decreasing transfer efficiencies. Furthermore, the presence of endogenous or covalently bound paramagnetic centers in the sample (Knight et al. 2012a; Laage et al. 2009; Nadaud et al. 2010), or the use of paramagnetic doping (Linser et al. 2009; Wickramasinghe et al. 2007, 2009) could also be used to increase sensitivity.

Overall, for systems where material is limited, or for which only de novo chemical shift assignments are needed, 1.3 mm rotors spinning at 60 kHz offer obvious advantages. For systems where the full assignment suite is not required, the additional signal seen in 2D and the less demanding 3D experiments using 1.9 mm rotors could prove advantageous. One context where this might be the case is multi-protein complexes, where solution NMR or ^{13}C -detected ssNMR provides assignments for one or more members of the complex. ^1H -detected NMR could then be used to detect differences in spectra of the protein in complex relative to those in a free solution. When considering the residues with the “worst” T_2 values, which may be expected from most protein systems of biological

interest, ^1H -dilution through back-exchange to 60 % yielded the most benefits, and might be warranted at higher spinning rates. Moreover, since the 1.9 mm probe was about five times more sensitive in 1D ^{13}C -detected experiments than the 1.3 mm probe, the 1.9 mm probe is likely better suited for ^{13}C detected experiments on the same rotor as ^1H detected ones, perhaps for distance restraint collection or in the context of ^2H excitation in a proton deficient sample or protein region. This line of thought can be taken a step further by considering 3.2 mm rotors that have even more ^{13}C sensitivity due to even larger sample volumes. When only material amount and rf-efficiency are considered, a 3.2 mm rotor would be expected to be about 6 times as sensitive as a 1.3 mm module, while a 1.9 mm system would be 2.5 times as sensitive, slightly higher than what we saw here experimentally for (H)NH 2Ds of SH3. After factoring in the 30 and 60 % back-exchange percentages, which allow for the same resolution for 3.2 and 1.9 mm rotors respectively, this factor would fall to 1.8 or 1.5, again slightly higher than what was seen here or in other work cited in the introduction. Keeping in mind that shorter T_2 times, especially for ^{13}C , caused C–C transfers to be less efficient at 40 kHz relative to 60 kHz, we expect that the faster spinning 1.9 and 1.3 mm rotors would be more sensitive for (H)C(C)NH-type experiments than 3.2 mm rotors. In summary, the larger rotors will always be slightly more sensitive for 1D or maybe even 2D experiments, however, the more transfer steps involved the larger the advantage of using smaller rotors will become.

Acknowledgments We would like to thank Matthias Hiller and Sebastian Wegner for assistance installing and calibrating the probes in Berlin. A.J.N. was supported by fellowships from the Fulbright Program and the Alexander von Humboldt Foundation. This work was also supported by the CNRS (TGIR-RMN-THC FR3050) and from a Joint Research Activity in the 7th Framework program of the EC (BioNMR No. 261863).

References

- Agarwal V et al (2014) De Novo 3D structure determination from sub-milligram protein samples by solid-state 100 kHz MAS NMR spectroscopy. *Angew Chem Int Ed Engl*. doi:10.1002/anie.201405730
- Akbe U et al (2010) Optimum levels of exchangeable protons in perdeuterated proteins for proton detection in MAS solid-state

- NMR spectroscopy. *J Biomol NMR* 46:67–73. doi:10.1007/S10858-009-9369-0
- Akbey U et al (2014) Quadruple-resonance magic-angle spinning NMR spectroscopy of deuterated solid proteins. *Angew Chem Int Ed Engl* 53:2438–2442. doi:10.1002/anie.201308927
- Asami S, Szekely K, Schanda P, Meier BH, Reif B (2012) Optimal degree of protonation for ^1H detection of aliphatic sites in randomly deuterated proteins as a function of the MAS frequency. *J Biomol NMR* 54:155–168. doi:10.1007/s10858-012-9659-9
- Baldus M, Petkova AT, Herzfeld J, Griffin RG (1998) Cross polarization in the tilted frame: assignment and spectral simplification in heteronuclear spin systems. *Mol Phys* 95:1197–1207
- Barbet-Massin E et al (2013) Out-and-back C–C scalar transfers in protein resonance assignment by proton-detected solid-state NMR under ultra-fast MAS. *J Biomol NMR*. doi:10.1007/s10858-013-9757-3
- Barbet-Massin E et al (2014) Rapid proton-detected NMR assignment for proteins with fast magic angle spinning. *J Am Chem Soc* 136:12489–12497. doi:10.1021/ja507382j
- Bockmann A et al (2009) Characterization of different water pools in solid-state NMR protein samples. *J Biomol NMR* 45:319–327. doi:10.1007/s10858-009-9374-3
- Chevelkov V et al (2003) ^1H detection in MAS solid-state NMR Spectroscopy of biomacromolecules employing pulsed field gradients for residual solvent suppression. *J Am Chem Soc* 125:7788–7789. doi:10.1021/ja029354b
- Chevelkov V, Faelber K, Diehl A, Heinemann U, Oschkinat H, Reif B (2005) Detection of dynamic water molecules in a microcrystalline sample of the SH3 domain of α -spectrin by MAS solid-state NMR. *J Biomol NMR* 31:295–310. doi:10.1007/S10858-005-1718-Z
- Chevelkov V, Rehbein K, Diehl A, Reif B (2006) Ultra-high resolution in proton solid-state NMR spectroscopy at high levels of deuteration. *Angew Chem Int Ed* 45:3878–3881. doi:10.1002/anie.200600328
- Chevelkov V, Habenstein B, Loquet A, Giller K, Becker S, Lange A (2014) Proton-detected MAS NMR experiments based on dipolar transfers for backbone assignment of highly deuterated proteins. *J Magn Reson* 242:180–188. doi:10.1016/j.jmr.2014.02.020
- Hediger S, Meier BH, Ernst RR (1993) Cross-polarization under fast magic-angle sample-spinning using amplitude-modulated spin-lock sequences. *Chem Phys Lett* 213:627–635. doi:10.1016/0009-2614(93)89172-E
- Huber M, Hiller S, Schanda P, Ernst M, Bockmann A, Verel R, Meier BH (2011) A proton-detected 4D solid-state NMR experiment for protein structure determination. *ChemPhysChem* 12:915–918. doi:10.1002/cphc.201100062
- Huber M, With O, Schanda P, Verel R, Ernst M, Meier BH (2012) A supplementary coil for $(2)\text{H}$ decoupling with commercial HCN MAS probes. *J Magn Reson* 214:76–80. doi:10.1016/j.jmr.2011.10.010
- Kay LE, Ikura M, Tschudin R, Bax A (1990) 3-Dimensional triple-resonance NMR-spectroscopy of isotopically enriched proteins. *J Magn Reson* 89:496–514. doi:10.1016/0022-2364(90)90333-5
- Knight MJ et al (2011) Fast resonance assignment and fold determination of human superoxide dismutase by high-resolution proton-detected solid-state MAS NMR spectroscopy. *Angew Chem Int Ed* 50:11697–11701. doi:10.1002/anie.201106340
- Knight MJ, Felli IC, Pierattelli R, Bertini I, Emsley L, Herrmann T, Pintacuda G (2012a) Rapid measurement of pseudocontact shifts in metalloproteins by proton-detected solid-state NMR spectroscopy. *J Am Chem Soc* 134:14730–14733. doi:10.1021/ja306813j
- Knight MJ et al (2012b) Structure and backbone dynamics of a microcrystalline metalloprotein by solid-state NMR. *Proc Natl Acad Sci USA* 109:11095–11100. doi:10.1073/pnas.1204515109
- Laage S, Sachleben JR, Steuernagel S, Pierattelli R, Pintacuda G, Emsley L (2009) Fast acquisition of multi-dimensional spectra in solid-state NMR enabled by ultra-fast MAS. *J Magn Reson* 196(133–141):2008. doi:10.1016/J.Jmr.10.019
- Lewandowski JR, Sein J, Sass HJ, Grzesiek S, Blackledge M, Emsley L (2010) Measurement of site-specific ^{13}C spin-lattice relaxation in a crystalline protein. *J Am Chem Soc* 132:8252–8254. doi:10.1021/ja102744b
- Lewandowski JR, Dumez JN, Akbey U, Lange S, Emsley L, Oschkinat H (2011) Enhanced resolution and coherence lifetimes in the solid-state NMR spectroscopy of perdeuterated proteins under ultrafast magic-angle spinning. *J Phys Chem Lett* 2:2205–2211. doi:10.1021/jz200844n
- Linsler R, Fink U, Reif B (2008) Proton-detected scalar coupling based assignment strategies in MAS solid-state NMR spectroscopy applied to perdeuterated proteins. *J Magn Reson* 193(89–93):2008. doi:10.1016/J.Jmr.04.021
- Linsler R, Fink U, Reif B (2009) Probing surface accessibility of proteins using paramagnetic relaxation in solid-state NMR spectroscopy. *J Am Chem Soc* 131:13703–13708. doi:10.1021/Ja903892j
- Linsler R, Fink U, Reif B (2010) Assignment of dynamic regions in biological solids enabled by spin-state selective NMR experiments. *J Am Chem Soc* 132:8891–8893. doi:10.1021/ja102612m
- Linsler R et al (2014) Solid-state NMR structure determination from diagonal-compensated, sparsely nonuniform-sampled 4D proton–proton restraints. *J Am Chem Soc* 136:11002–11010. doi:10.1021/Ja504603g
- Marchetti A et al (2012) Backbone assignment of fully protonated solid proteins by ^1H detection and ultrafast magic-angle-spinning NMR spectroscopy. *Angew Chem Int Ed* 51:10756–10759. doi:10.1002/anie.201203124
- Nadaud PS, Helmus JJ, Sengupta I, Jaroniec CP (2010) Rapid acquisition of multidimensional solid-state NMR spectra of proteins facilitated by covalently bound paramagnetic tags. *J Am Chem Soc* 132:9561–9563. doi:10.1021/Ja103545e
- Reif B, Jaroniec CP, Rienstra CM, Hohwy M, Griffin RG (2001) ^1H – ^1H MAS correlation spectroscopy and distance measurements in a deuterated peptide. *J Magn Reson* 151:320–327. doi:10.1006/jmre.2001.2354
- Shaka AJ, Keeler J, Frenkiel T, Freeman R (1983) An improved sequence for broad-band decoupling—Waltz-16. *J Magn Reson* 52:335–338. doi:10.1016/0022-2364(83)90207-X
- Stevens TJ et al (2011) A software framework for analysing solid-state MAS NMR data. *J Biomol NMR* 51:437–447. doi:10.1007/s10858-011-9569-2
- van Rossum BJ, Castellani F, Rehbein K, Pauli J, Oschkinat H (2001) Assignment of the nonexchanging protons of the α -spectrin SH3 domain by two- and three-dimensional ^1H – ^{13}C solid-state magic-angle spinning NMR and comparison of solution and solid-state proton chemical shifts. *ChemBioChem* 2:906–914. doi:10.1002/1439-7633(20011203)2:12<906:AID-CBIC906>3.0.CO;2-M
- Verel R, Ernst M, Meier BH (2001) Adiabatic dipolar recoupling in solid-state NMR: the DREAM scheme. *J Magn Reson* 150:81–99. doi:10.1006/jmre.2001.2310
- Ward ME, Shi L, Lake E, Krishnamurthy S, Hutchins H, Brown LS, Ladizhansky V (2011) Proton-detected solid-state NMR reveals intramembrane polar networks in a seven-helical transmembrane protein proteorhodopsin. *J Am Chem Soc* 133:17434–17443. doi:10.1021/ja207137h
- Ward ME, Wang S, Krishnamurthy S, Hutchins H, Fey M, Brown LS, Ladizhansky V (2014) High-resolution paramagnetically

- enhanced solid-state NMR spectroscopy of membrane proteins at fast magic angle spinning. *J Biomol NMR* 58:37–47. doi:[10.1007/s10858-013-9802-2](https://doi.org/10.1007/s10858-013-9802-2)
- Wickramasinghe NP, Kotecha M, Samoson A, Past J, Ishii Y (2007) Sensitivity enhancement in ^{13}C solid-state NMR of protein microcrystals by use of paramagnetic metal ions for optimizing ^1H ^1T relaxation. *J Magn Reson* 184:350–356. doi:[10.1016/j.jmr.2006.10.012](https://doi.org/10.1016/j.jmr.2006.10.012)
- Wickramasinghe NP et al (2009) Nanomole-scale protein solid-state NMR by breaking intrinsic ^1H ^1T boundaries. *Nat Methods* 6:215–218. doi:[10.1038/Nmeth.1300](https://doi.org/10.1038/Nmeth.1300)
- Zhou DH, Rienstra CM (2008) High-performance solvent suppression for proton detected solid-state NMR. *J Magn Reson* 192:167–172. doi:[10.1016/j.jmr.2008.01.012](https://doi.org/10.1016/j.jmr.2008.01.012)
- Zhou DH, Graesser DT, Franks WT, Rienstra CM (2006) Sensitivity and resolution in proton solid-state NMR at intermediate deuteration levels: quantitative linewidth characterization and applications to correlation spectroscopy. *J Magn Reson* 178:297–307. doi:[10.1016/j.jmr.2005.10.008](https://doi.org/10.1016/j.jmr.2005.10.008)
- Zhou DH, Shah G, Cormos M, Mullen C, Sandoz D, Rienstra CM (2007a) Proton-detected solid-state NMR spectroscopy of fully protonated proteins at 40 kHz magic-angle spinning. *J Am Chem Soc* 129:11791–11801. doi:[10.1021/ja073462m](https://doi.org/10.1021/ja073462m)
- Zhou DH et al (2007b) Solid-state protein-structure determination with proton-detected triple-resonance 3D magic-angle-spinning NMR spectroscopy. *Angew Chem Int Ed Engl* 46:8380–8383. doi:[10.1002/anie.200702905](https://doi.org/10.1002/anie.200702905)
- Zhou DH et al (2012) Solid-state NMR analysis of membrane proteins and protein aggregates by proton detected spectroscopy. *J Biomol NMR* 54:291–305. doi:[10.1007/s10858-012-9672-z](https://doi.org/10.1007/s10858-012-9672-z)